Available online at www.sciencedirect.com
ScienceDirect
Journal of Power Sources 168 (2007) 126–134
JOURNAL OF POWER SOURCES
www.elsevier.com/locate/jpowsour

Relationships between microstructure and transport properties of proton-conducting porous PVDF membranes

Eliana Quartarone [a,*], Arianna Carollo [a], Corrado Tomasi [b], Federico Belotti [a], Stefania Grandi [a], Piercarlo Mustarelli [a], Aldo Magistris [a]

[a] *Department of Physical Chemistry and INSTM, University of Pavia, Via Taramelli 16, 27100 Pavia, Italy*
[b] *IENI-CNR, Via Taramelli 16, 27100 Pavia, Italy*

Received 16 October 2006; received in revised form 21 February 2007; accepted 24 February 2007
Available online 12 March 2007

Abstract

Fluorinated polymers are today investigated as possible alternatives to Nafion™ in PEM Fuel Cells. In this paper, we study the relationships between the microstructure and the proton transport of porous PVDF homopolymer membranes swollen by 11 M aqueous solution of H_3PO_4. The analysis is performed on membranes with different nominal pores size values, d_p. The membranes are thermally stable at least up to 250 °C. A dependence of the proton transport on the pores size has been found, that is particularly evident for low d_p values and at low relative humidity (R.H.). Conductivity values exceeding 0.1 S cm^{-1} are obtained at 80 °C even at 10% R.H. for $d_p \geq 0.22$ μm. We show that the behaviour of the transport properties cannot be simply rationalized in terms of d_p, but it requires an accurate knowledge of the membrane microstructure (tortuosity, pores interconnections and size distributions). ^{31}P NMR spectroscopy also shows that anisotropic interactions take place between the components of the solution and at a lower extent, between the solution and the pores walls, also for d_p values in the micrometer range. In order to make a preliminary check of the suitability of these membranes for applications in Direct Methanol Fuel Cells (DMFCs), studies of methanol crossover and diffusion through the membrane have been carried out and compared with those of Nafion™.

Keywords: Fuel cells; Polymer electrolytes; Proton conductivity; Microstructure; NMR; AFM

1. Introduction

The search for new proton-conducting membranes as possible alternatives to Nafion™ is rapidly growing. Fluorinated polymers are particularly appealing because of their chemical and physical affinity with Nafion™ [1]. Unfortunately, such polymers are hydrophobic in nature and must be chemically modified, e.g. by means of radiation grafting, in order to gain hydrophilic properties. Systematic investigations on this kind of PVDF- and PTFE-based polymers were carried out mainly by Scherer and co-workers [2–6] and by Sundholm and co-workers [7,8]. A bulk of information on synthesis [9], electrochemical performances [10–13] and microstructure modifications with respect to the pristine polymers [14,15] is now available in literature. The topic has been recently reviewed [16].

During the last decade, several studies have shown the suitability of PVDF-based porous films, swollen with lithium-based organic liquid electrolytes, as separators in lithium batteries [17,18]. The strengths of these materials are low-cost synthesis, good mechanical and chemical resistances, and large liquid uptakes that give a liquid-like conductivity. Recently, a similar approach has been used by Peled et al. [19], and successively by Scrosati and co-workers [20,21], in order to test PVDF as a proton-conducting material. The basic idea is to prepare porous membranes by means of the well proved phase inversion technique [22], and to fill them with an aqueous highly concentrated acid solution, using for instance H_3PO_4 or H_2SO_4. Quite thermally stable membranes with proton conductivity up to 0.2 S cm^{-1} at room temperature have been easily obtained, whose proton transport only slightly depends on the humidity conditions. However, it should be stressed out that the use of

* Corresponding author. Tel.: +39 0382 987894; fax: +39 0382 987895.
E-mail address: elena.quartarone@unipv.it (E. Quartarone).

0378-7753/$ – see front matter © 2007 Elsevier B.V. All rights reserved.
doi:10.1016/j.jpowsour.2007.02.082

acid-loaded porous membranes in a fuel cell may be flawed because of the lack of strong physico/chemical interactions between the host polymer and the electrolyte phase, which causes liquid leakage. On the other hand, this problem can be overcome by fabricating (nano)composite systems with passive or active fillers [23,24], or even by preparing blends with other polymers [21].

In order to develop efficient strategies for the designing of new nano-composite materials based on porous polymer matrices, it is important to have an accurate knowledge of the membrane microstructure (pore size and pore size distribution, open volume, pores interconnections, tortuosity), as well as of the interactions taking place among the conducting liquid phase and the pore walls. While phase-inverted porous PVDF films with different microstructure and properties can be prepared in the laboratory, a good model system may be given by commercially available membranes for micro- and ultrafiltration. In this paper, we report a careful physico-chemical study of the transport properties of porous PVDF commercial membranes swollen by 11 M aqueous solution of H_3PO_4. Here, the main advantage is related to the commercial availability of hydrophilic films which do not need any chemical modification of their surface of bulk in order to be activated with the electrolyte solution. Our chief aim is to correlate the membranes microstructure with the electrolyte transport properties, in order to establish a good starting point to develop strategies for effective liquid confinement. In order to make a preliminary check of the suitability for application in Direct Methanol Fuel Cells (DMFCs), studies of methanol crossover and diffusion have been carried out and compared with those of Nafion™.

2. Experimental

Durapore™ hydrophilic PVDF membranes (Millipore) of four different nominal pore sizes, $d_p = 0.1$, 0.22, 0.65 and 5 μm, were used as the polymer hosts. The membranes were chemically modified (industrial secret) by the provider in order to be hydrophilic. The reported nominal porosity and thickness of the membranes were 70% and 120 μm, respectively. The PVDF films were immersed in an aqueous solution of H_3PO_4 (85 wt%) for 24 h and gently dried with an absorbing paper before the measurements. The resulting volume uptakes are reported in Table 2.

The average pore size and the pores distribution of the as-received membranes were obtained with an Autoprobe CP microscope (ThermoMicroscopes-VEECO), operating in tapping mode (TM-AFM), by means of sharpened silicon tip onto rectangular-shaped cantilevers (resonance frequency, 150 kHz; force constant, 5.5 N m^{-1}). For each analysed membrane, scans of 50 μm × 50 μm and 15 μm × 15 μm have been carried out with a scan rate ranging from of 0.5 to 0.7 Hz. A standard second order flatten processing of the images has been performed in order to correct the scanner non-linearity. The bi-dimensional 15 μm × 15 μm images have been analysed by means of the Jandel® ScanPro 5.0 software. Each photograph was digitized with a resolution of 1024 × 768 pixels, and the pores sizes (∼50 objects) were stored in a worksheet in order to be plotted as histograms. For more details see Ref. [25].

^{31}P static and Magic Angle Spinning (MAS) NMR spectra were acquired at room temperature with a AMX400WB spectrometer (Bruker), equipped with a 7 mm MAS probe (Bruker), at the Larmor frequency of 161.98 MHz. A single-pulse sequence was used with a 90° pulse of 4 μs, and a delay time of 5 s. Twenty-four scans were enough to obtain a good signal-to-noise ratio. The MAS spectra were obtained at several spinning frequencies in the range from 100 Hz to 7 kHz.

Scanning Electron Microscopy images of the samples were taken by means of a variable pressure Scanning Electron Microscope VEGA TS 5136 (Vega-Tescan) using an accelerating voltage of 10 kV and achieving magnifications ranging from 4000 to 14,300.

The DSC measurements were performed with a 2910 MDSC (TA Instruments) by using silver pans, at a rate of 5 °C min^{-1} under nitrogen purge. TGA scans were also recorded at 5 °C min^{-1} under nitrogen flow with a 2950 TGA (TA Instruments). We also performed isothermal TGA experiments at 80 °C and 40% R.H.

The proton conductivity was measured by means of the impedance spectroscopy technique, using a frequency response analyser (FRA Solartron 1255), connected to an electrochemical interface (Solartron 1287), over the frequency range 1 Hz–1 MHz, by applying a voltage of 100 mV. The membrane was fixed to a four-points measure cell put in a homemade climatic chamber. The check of the operating conditions (sample temperature and relative humidity) was performed by means of a thermo-hygrometric probe (Rotronic AG). The impedance scans were performed with the following protocols: (i) at room temperature ranging from 0 to 100% R.H.; (ii) at 80 °C ranging from 10 to 50% R.H. and (iii) by varying the temperature from room temperature to 70–80 °C at the constant moisture level of 40% R.H. The films were allowed to equilibrate for 3–4 h at each moisture level before the measurements; longer equilibration times were allowed in some selected cases that did not show further changes of the conductivity. A rough idea of the long-term stability under humidity conditions similar to those that could be expected in a fuel cell working at low R.H. was obtained by keeping the 0.22 μm membrane at 80 °C and 40% R.H. for 250 h. Conductivity variations lower than 6% were observed.

The methanol permeation rate through the membrane was determined at 25 °C by using a standard split cell. The membranes (surface area of 4.9 cm^2) were vertically placed between two sections of identical volume (37 cm^3) containing a solution of methanol 0.2 M and deionized water, respectively. The cell was magnetically stirred so that methanol can reach the equilibrium on both chambers. Small aliquots of 1 μL were taken at different times in the water reservoir, and the methanol concentration was measured by means of a gas chromatograph equipped with a flame ionization detector (Perkin Elmer Clarus 500). The possible dissolution of phosphoric acid in the methanol was not considered.

3. Results and discussions

3.1. Microstructural characterization of the membranes as-received

The nominal pore size, d_p, of the Durapore™ membranes is defined as the diameter of the largest accessible pore, as determined by the so-called "bubble point test" [26]. Within this test, the minimum pressure required to force liquid from the capillary structure is directly related to the capillary diameter. However, the pore size distribution and other topological/microstructural parameters (tortuosity, pore shape, etc.) are likely more relevant than d_p in determining the overall technological properties of the membrane. Fig. 1 shows, as an example, the SEM picture of the membrane 0.65 μm. It is easy to observe that the microstructure of the film is complex, and hardly interpretable in terms of the nominal pore size. More detailed information can be obtained from the micrographs by means of standard image analysis techniques.

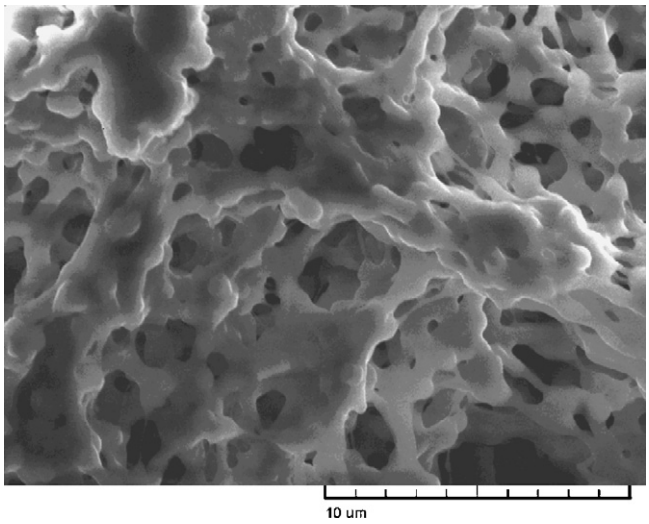

Fig. 1. SEM picture of the membrane with 0.65 μm nominal pore size.

Fig. 2 shows the AFM pictures of all the membranes, from which it is possible to obtain information on the surface roughness, as well as on surface density, shape and interconnections of the pores. Table 1 reports the values of the surface pore density, N_p, surface porosity, ε_s, and surface roughness, R_{rms} (see Ref. [27]). All these parameters display non-linear behaviours as a function of d_p. In particular the former two, which are obviously correlated, show maxima for $d_p = 0.22$ μm, whereas the third one attains a local minimum for the same membrane. Fig. 3 shows the behaviours of the tortuosity, defined as $\tau = \varepsilon/\varepsilon_s$, where ε is the nominal porosity, and of the pore shape factor, $s_p = 4\pi A_p/P_p^2$, that is the ratio between the actual pore area

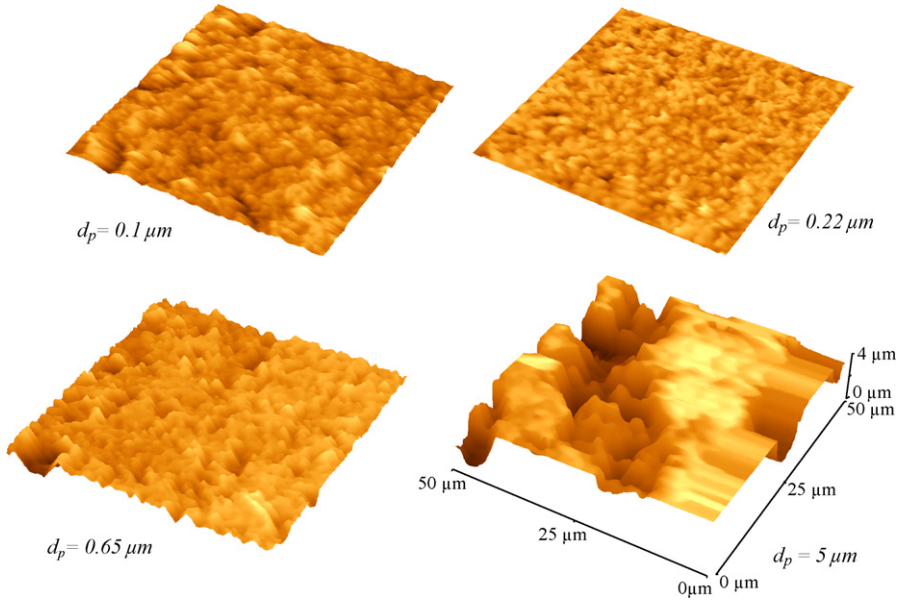

Fig. 2. 3D AFM pictures (50 μm × 50 μm) of all the membranes.

Table 1
Morphological properties of the as-received membranes

Membrane, d_p	t (μm)	ε (%)	N_p (10^{11} m^{-2})	ε_s (%)	R_{rms} (μm)	f_{max} (%)	μ (μm)	σ (μm)	m_1 (μm)	M_2 (μm^2)	M_3 (μm^3)
0.1	125	70	1.10	1.63	0.37	25.4 ± 3.7	0.21 ± 0.02	0.55 ± 0.07	0.34_5	0.07	0.038
0.22	125	70	2.30	13.70	0.20	14.2 ± 1.5	0.24 ± 0.02	0.72 ± 0.07	0.64	0.34	0.278
0.65	125	70	0.70	3.25	0.48	11.6 ± 1.9	0.29 ± 0.07	1.15 ± 0.25	0.62	0.19_5	0.175
5.0	125	70	0.05	2.35	2.28	6.85 ± 1.0	1.14 ± 0.26	0.92 ± 0.32	1.66	2.66	18

t, nominal thickness; ε, nominal porosity; N_p, surface pore density by AFM; ε_s, surface porosity by AFM; R_{rms}, surface roughness by AFM; f_{max}, μ and σ, best fit values of Eq. (1); m_1, pores size mean; M_i, moments of the distribution (see Eq. (2)).

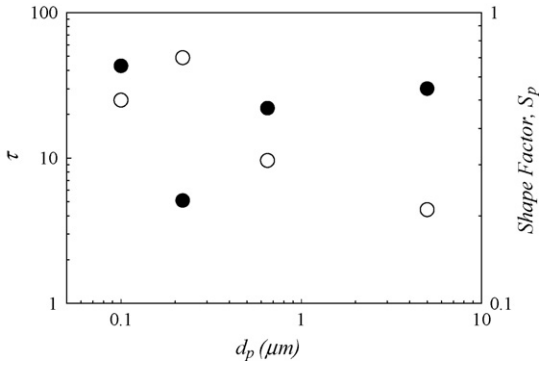

Fig. 3. Behaviour of tortuosity, τ (filled circles), and pores shape factor, s_p (open circles), vs. d_p.

and the corresponding area of a circle with the same perimeter. Within these definitions, the tortuosity measures the pores interconnections and chiefly the openings at the surface, whereas the shape factor is related to the pore symmetry. In particular, $s_p = 1$ is obtained for a pore of circular section (spherical or even cylindrical symmetry). The membrane 0.22 μm is characterized by a minimum of the tortuosity, and by a maximum of the shape factor of the surface pores, whose value is near to the unity. On this basis, this membrane seems the best suited from the point of view of the use in a fuel cell. Our tortuosity value of 5.1 is nearly double than that reported in Ref. [27] for the same membrane, which on the other hand, was obtained on smaller scanned areas. We stress that other ways to define the tortuosity of a membrane are possible [18]. However, also the capability to retain the liquid phase should be considered for technological applications in PEMFCs. This point will be addressed in Section 3.5.

Indeed, also the pores size distribution may play a relevant role in determining the transport properties of the membrane. Fig. 4 shows the pores size distributions obtained from the AFM pictures as described in Section 2. The histograms have been best fitted with a standard log–normal distribution function [25]

$$f = f_{\max}\, e^{-(\ln(x/\mu))^2/2\sigma^2} \quad (1)$$

where $f_{\max}$ is the maximum of f, μ the most probable value of x and σ^2 is the usual variance. The best-fitting results are reported

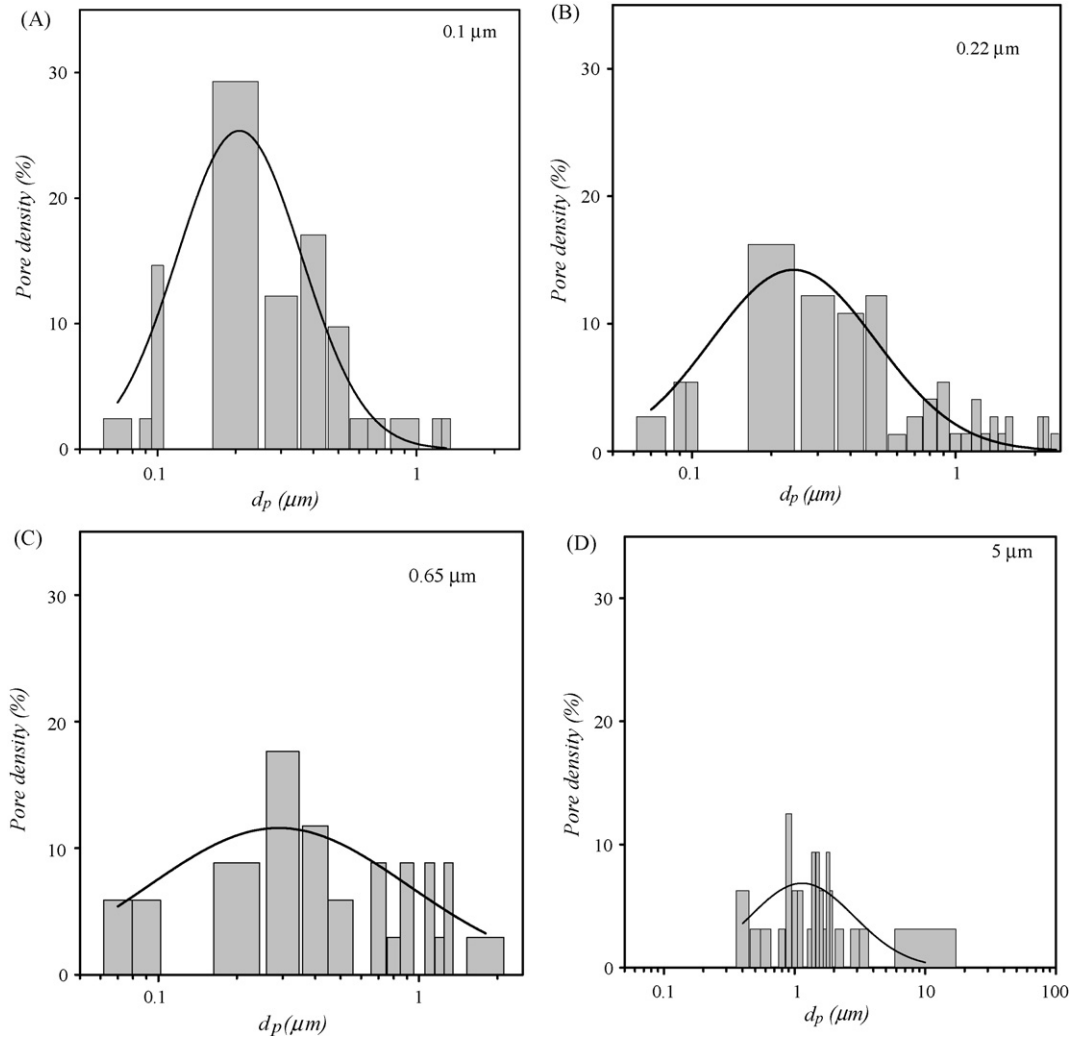

Fig. 4. Histograms of the pores size distributions as obtained by the AFM picture (see text); d_p, 0.1 μm (A); d_p, 0.22 μm (B); d_p, 0.65 μm (C); d_p, 5 μm (D). The continuous lines are the best fits with the log–normal distribution (Eq. (1)).

Table 2
Volume uptake, transport and diffusion properties of the activated membranes

Membrane	d_p (μm)	T (μm)	$\Delta\Phi$ (%)	ε_v (%)	$\sigma_{80\,°C/R.H.=40\%}$ (mS cm^{-1})	E_a (eV)	DK (10^{-6} cm^2 s^{-1})
PVDF	0.1	125	<1	65	80	$0.13_5 \pm 0.014$	1.8
PVDF	0.22	125	<1	62	120	0.13 ± 0.013	3.4
PVDF	0.65	125	<1	62	100	0.05 ± 0.006	3.7
PVDF	5	121	<1	61	80	0.06 ± 0.005	1.9
Nafion™ 117	–	175[a]	13	45	2.9	–	1.0

T, thickness after immersion; $\Delta\Phi$, swelling; ε_v, volume uptake (Eq. (3)); σ, ionic conductivity; E_a, activation energy for conductivity; D, methanol self-diffusion coefficient.
[a] From the supplier.

in Table 1, together with the nominal values of some properties given by the supplier. The best fits are not satisfactory, most of all in the case of the membranes with larger pores, because of the difficulty in reconstructing the histograms. More reliable information can be obtained by re-elaborating the histograms data, x_i, in terms of normalized moments, M_k, which are usually defined as

$$M_k = \sum_{i=1}^{N} p_i (x_i - m_1)^k \quad (2)$$

Here, the p_i is the normalized weight of the distribution, and m_1 is its mean. Under these assumptions, the moment $k=2$ is the usual variance, and the moment $k=3$ is an asymmetry index of the distribution. The M_k values are reported in Table 1. Both M_2 and M_3 display a local maximum for $d_p = 0.22$ μm, which means that this membrane is characterized by a pores size distribution wider and more asymmetric than that of $d_p = 0.1$ μm and $d_p = 0.65$ μm membranes. Of course, the abovementioned conclusions are taken under the assumption that the pore size distribution is uniform across the sample section, which is reasonable for symmetric membranes.

3.2. The uptake of the acid solution

Table 2 reports the volume uptake of the membranes, calculated with the following relationship:

$$\varepsilon_v = \frac{V_{liq}}{V_T} = \frac{(w_{wet} - w_{dry}) \times \rho_{dry}}{(w_{wet} - w_{dry}) \times \rho_{dry} + w_{dry} \times \rho_{sol}} \quad (3)$$

where $(w_{wet} - w_{dry})$ is the weight of the liquid absorbed by the membrane, ρ_{sol} and ρ_{dry} are the densities of the aqueous solution and of the dried membrane, respectively.

The liquid uptake ranges from 61 to 65%, depending on the membrane d_p, which is in reasonable agreement with the nominal porosity of 70%. This confirms that the pores are almost completely interconnected, and that the acid solution does not swell the polymer domains, contrary to what is generally observed in the case of Nafion™ [28]. On the other hand, this must be expected because PVDF, contrary to Nafion™, has not in its structure covalently bonded acid moieties to be solvated and also, although to a less extent, because PVDF is normally more crystalline than Nafion™ itself.

3.3. Thermal properties

Fig. 5 shows the TGA curves of the as-received PVDF membrane with $d_p = 0.1$ μm (a) and of the H_3PO_4 85 wt% aqueous solution (b). As expected, the untreated membrane is stable up to ~450 °C. The acid solution displays an initial weight loss up to ~100 °C that is related to the removal of the solution water. The following monotonic loss, up to ~500 °C can be attributed to the progressive condensation of the H_3PO_4 units to give polyphosphoric moieties. The further weight decrease above ~500 °C is likely due to the evaporation of the condensed units.

The DSC and TGA curves of the activated membranes are reported in Figs. 6 and 7, respectively. Each DSC curve shows a broad endotherm ranging from room temperature up to ~130 °C, corresponding to the weight loss recorded in the TGA trace in the same temperature range. Between 160 and 180 °C all the curves present an endothermic DSC peak due the polymer melting. Near 300 °C exothermic features appear that are due to the samples decomposition, as demonstrated by the weight losses showed by the TGA signals in the same temperature range. Interestingly, the membrane with $d_p = 5$ μm shows two exotherms at ~260 and ~300 °C that correspond to the two-stages degradation losses probed by TGA. A careful analysis of the above figures allows one to make two other remarks, which may be relevant in order to understand the interactions between the polymer matrix and the solution components:

(i) The temperature range of water release seems to be shifted towards high temperatures by increasing the pores size,

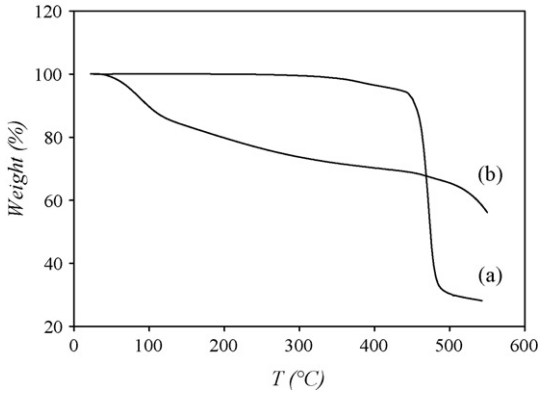

Fig. 5. TGA curves of the PVDF membrane (as-received) with 0.1 μm pores size (a) and of the H_3PO_4 85 wt% aqueous solution (b).

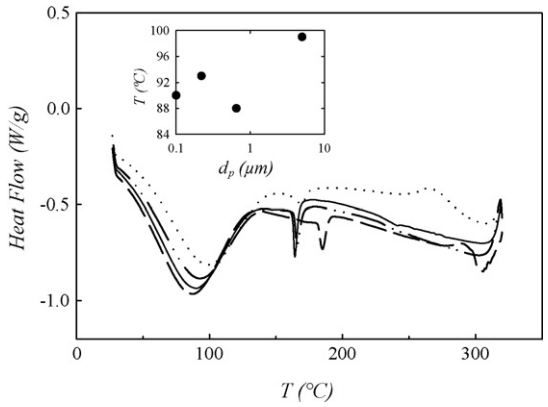

Fig. 6. DSC traces of the PVDF-based membranes activated with the H_3PO_4 solution, for different pores size; d_p, 0.1 μm (solid line); 0.22 μm (dash-dot-dot line); 0.65 μm (dashed line); 5 μm (dotted line). The inset shows the temperature of the minimum of the water loss endotherm vs. the pores size (see text).

with the possible exception of $d_p = 0.65$ μm. This fact is more evident in the DSC traces (see inset of Fig. 6), and can be rationalized by supposing that the interactions among the solution molecules are stronger than those among water and PVDF, inspite of the hydrophilic nature of the membranes. Therefore, the different extent of the polymer/solution inter-phases, which depends on the pores size, can justify the shift in temperature. This interpretation is supported by the solid-state NMR results reported in Section 3.6.

(ii) The decomposition temperature recorded for the activated membranes is much lower than those of the corresponding as-received ones (see Fig. 5), which means that the interactions of the polymer backbone with the phosphoric acid are important in promoting the samples degradation. Interestingly, the decomposition temperature of the activated membranes decreases as the pores size increases (see inset in Fig. 7). Since these results are based on a dynamic TGA, it may be just the easier release of the decomposition products which lead to the observed differences.

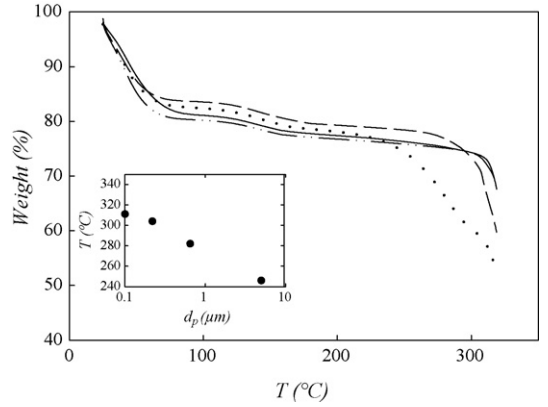

Fig. 7. TGA curves of the PVDF-based membranes activated with the H_3PO_4 solution; d_p, 0.1 μm (solid line); 0.22 μm (dash-dot-dot line); 0.65 μm (dashed line); 5 μm (dotted line). The inset shows the degradation temperature vs. the pores size (see text).

Both these facts, in any case, are a first evidence that physico-chemical interactions take place between the electrolyte solution and the polymer strands, and that these interactions somehow depend on the nominal pores size and/or on microstructural parameters like tortuosity and pores size distribution. In Section 3.5 this aspect will be further investigated from a microscopic point of view. Finally, we performed a rough check of the thermal stability of the membrane with $d_p = 0.22$ μm at 80 °C and 40% R.H. We registered a weight loss lower than 0.5% over 10 days, which is of the same order of the instrumental drift.

3.4. Methanol crossover

The methanol transport across a membrane is generally determined by assuming molecular diffusion as predicted by Fick's law. In the case of porous media, this phenomenon is further complicated by morphological factors like pores structure and tortuosity. The relationship between the microstructure of the membrane and the methanol crossover has been developed by Verbrugge, by means of a model that quantitatively simulates the methanol transport experiments [29]. The methanol permeation across the membrane can be determined by acquiring the methanol concentration changes with time in the pure water reservoir, c_B, as per the following linear relationship:

$$c_B(t) = \frac{A}{V_B L} DK c_A (t - t_0) \quad (4)$$

here A and L are the membrane area and thickness, respectively, V_B the water chamber volume, c_A the initial methanol concentration, t_0 the "time lag" and D and K are the methanol diffusion and partition coefficients. The permeation rate, or permeability, DK, is extracted from the slope of Eq. (4) and reflects the changes in the diffusion coefficients, in the case of partition coefficients $K = 1$.

Fig. 8 shows the behaviour of the methanol concentration with time in the case of Nafion™ 117 and the PVDF films with $d_p = 0.1$ and 5 μm. The MeOH amount diffused through the membrane changes quasi-linearly as a function of the time. The

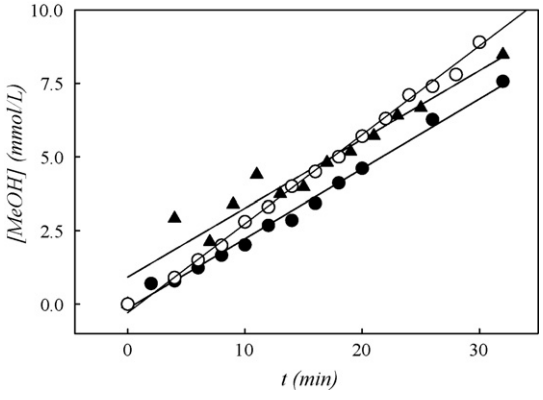

Fig. 8. Methanol concentration vs. time at room temperature in the case of two imbibed PVDF membranes: with $d_p = 0.1$ μm (filled circles) and $d_p = 5$ μm (filled triangles). The values of Nafion™ 117 (open circles), measured in the same experimental conditions, are reported for the sake of comparison. The lines are linear best fits.

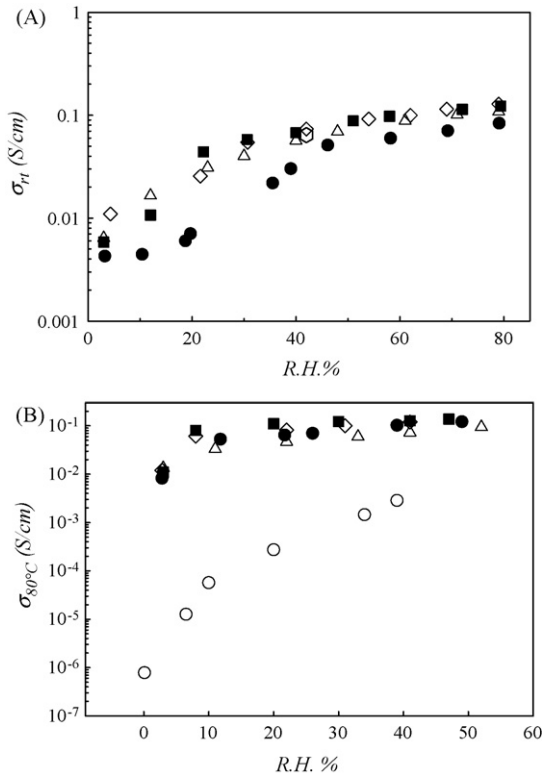

Fig. 9. (A) Proton conductivity at room temperature vs. the relative humidity for the PVDF-based membranes with different d_p: 0.1 μm (filled circles), 0.22 μm (filled squares), 0.65 μm (open diamonds) and 5 μm (open triangles). The conductivity value of the acid solution (open hexagon), measured under the same experimental conditions, is reported for the sake of comparison. (B) Proton conductivity vs. relative humidity at 80 °C for the same samples of (A). The conductivity values of Nafion^{TM} 117 are plotted for the sake of comparison (open circles).

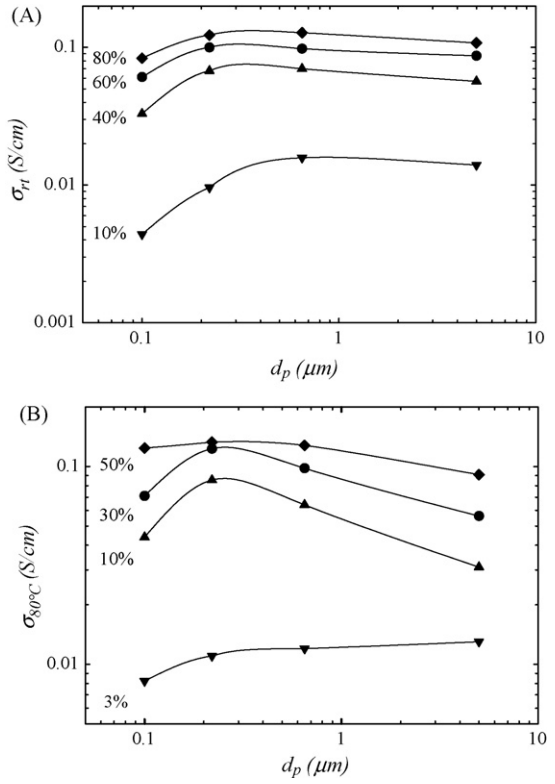

Fig. 10. Behaviour of the proton conductivity at room temperature (A) and 80 °C (B) as a function of the membrane pore size, d_p, at different relative humidity values (indicated as percentages in the figures). Some points are obtained by interpolation.

only significant dispersion is observed in the case of the 5 μm membrane for $t \leq 10$ min. The methanol crossover is slightly higher for the film with larger pore diameter. However, the pores diameter does not seem to affect greatly the methanol permeation rate.

The permeability values of the PVDF membranes are quite similar to that one we measured on Nafion^{TM} which, in turn, is in good agreement with that reported in the literature for similar film thickness and methanol concentration [30]. This result may be expected, if we take into account that the methanol crossover mechanism is assisted by the water domains into the pore regions and/or in the interconnecting channels of the membrane, where the methanol solubility is high [28].

3.5. The proton conductivity

Fig. 9A and B shows the conductivity behaviour versus R.H.% for all the membranes at room temperature and at 80 °C, respectively. At room temperature the proton conductivity increases with the moisture content from $\sim 4 \times 10^{-3}$ to $\sim 10^{-1}$ S cm^{-1}. In particular, at R.H. = 40% the conductivity of the membranes with $d_p \geq 0.22$ μm is well comparable with that of the acid solution (see caption). At 80 °C the influence of both the moisture level and the nominal pores size on the proton transport is less relevant, and values in the range 0.05–0.1 S cm^{-1} are already found for R.H. higher than 10%.

Fig. 10A and B shows the behaviour of the conductivity at room temperature and 80 °C versus the nominal pores size at different moisture levels. At both the temperatures, non-linear behaviours are observed in the log–log plots. In particular, at room temperature the conductivity describes very shallow maxima for $d_p = 0.22$–0.65. At 80 °C, in contrast, well-pronounced maxima are found at R.H. ≥ 10% for $d_p = 0.22$, i.e. for the membrane characterized by the best values of tortuosity and pores shape factor (see Fig. 3), and by the largest pores size distribution (see Table 1). On the other hand, this is in agreement with the expected relationships between transport properties and tortuosity in porous media [31]. Our results confirm that, as expected, the simple choice of the nominal pore size as the relevant parameter to state the goodness of a membrane is not satisfactory, and that more significant quantities must be searched for. However, the nominal pore size may retain some importance in order to allow comparisons among different products and suppliers.

Fig. 11 reports the behaviours of the proton conductivity versus the temperature at 40% R.H. In each case the logarithm of the conductivity increases linearly with the temperature. The Arrhenian activation energies, reported in Table 2, seem to decrease as d_p increases, except for the $d_p = 5$ μm where a slightly higher value is found. This trend can be explained in terms of a more extended continuity of the liquid phase in the membranes with higher pores diameters, which enables a

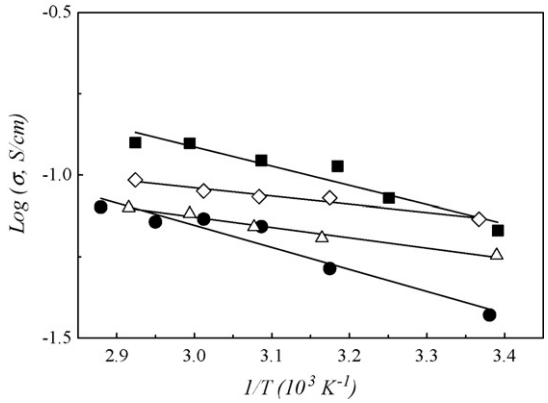

Fig. 11. Plot of the proton conductivity as a function of the temperature at 40% R.H. for the investigated PVDF-based membranes: $d_p = 0.1$ μm (filled circles); 0.22 μm (filled squares); 0.65 μm (open diamonds); 5 μm (open triangles).

better proton displacement. The membrane $d_p = 0.22$ μm shows the best values of the conductivity nearly all over the explored temperature region. In conclusion, we confirm that the transport properties of these membranes are chiefly determined by microstructure, and namely by pores shape, interconnections, and pores size distributions, rather than simply by the nominal pores size.

3.6. Solid-state NMR characterization of the matrix–solution interactions

Information on the interactions among the ionic solution and the polymer cage can be obtained by means of NMR spectroscopy [32]. In particular, ^{31}P is a good nuclear probe because of: (i) its spin, $I = 1/2$, which allows to extract chemical shift information, and (ii) its high isotopic abundance (100%) and magnetogyric ratio ($\gamma = 1.08 \times 10^8$ rad s^{-1} T^{-1}) which easily allow to obtain spectra with good signal-to-noise ratios. In our case, the overall static Hamiltonian, H_{TS}, determining the shape and width of the spectra can be written as

$$H_{TS} = H_z + H_{CS} + H_D + (\text{higher-order terms})$$

where H_z is the Zeeman term, H_{CS} the anisotropic chemical shift and H_D is the magnetic dipolar interaction among the phosphorous and the other NMR-active nuclei, which in our case are only ^{31}P and ^{1}H, since ^{13}C and ^{17}O can be neglected because of their low isotopic abundance. Fig. 12 shows the static and MAS spectra of the membrane $d_p = 5$ μm. The static spectrum displays a full width at half height (FWHH) of ∼345 Hz that is narrowed to ∼220 Hz under MAS conditions. While the static line is already narrowed by spin diffusion, the ∼35% further narrowing observed under MAS rotation is due to an additional averaging out of the anisotropic contributions of both H_{CS} and H_D. Therefore, we can conclude that, under static conditions, a non-negligible anisotropic interaction takes still place among each phosphorus and the other ^{31}P nuclei of the PO_4 groups and the ^{1}H nuclei of both the solution and the pore walls. In other words, also for the largest d_p we have at disposal, the solution behaves like a quasi-confined phase, probably because of the

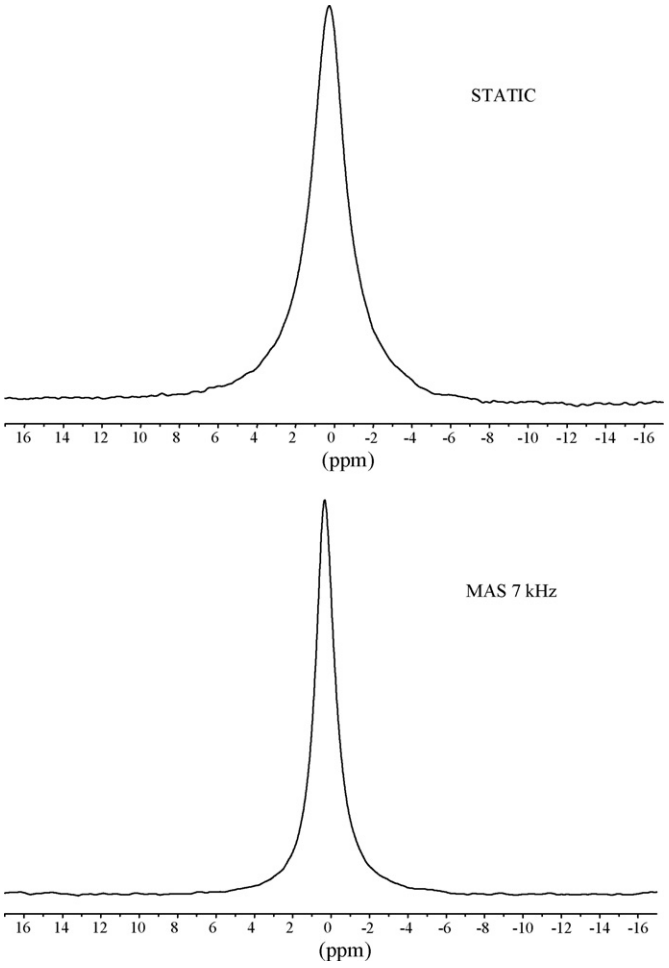

Fig. 12. Static (upper part) and MAS (lower part) ^{31}P NMR spectra of the membrane $d_p = 5$ μm.

width of the pores size distribution which includes pores in the nanometer range.

Fig. 13 shows the static and MAS line width values for all the matrices we studied. The static values increase quasi-linearly with d_p, which confirms that the interactions among the molecules inside the solution are more relevant than the solution–polymer ones in determining the line width, in agree-

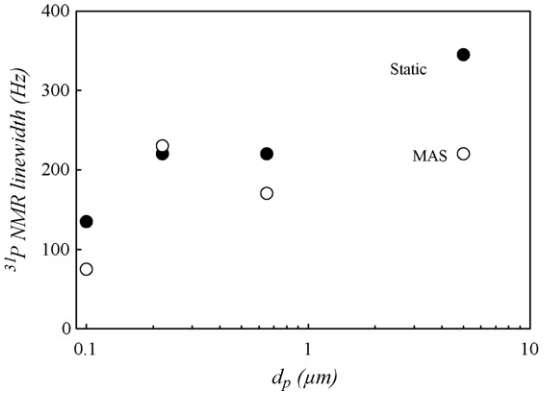

Fig. 13. Behaviour of the ^{31}P NMR line width vs. d_p for the static and MAS spectra.

ment with the DSC results of Fig. 6. The MAS values display a similar behaviour, with the notable exception of the membrane $d_p = 0.22\ \mu m$. In this case, in fact, the MAS rotation does not cause any further narrowing with respect to the static line, so suggesting that the interactions determining the static line width are already isotropic in nature (full narrowing regime). This calls for a high mobility of the ions (in the NMR timescale), in agreement with the observed values of the conductivity, and may be put into relation with the low tortuosity and the high shape factor values reported in Fig. 3.

4. Concluding remarks

In this paper we studied the microstructure, the functional properties and the solution–polymer interactions of porous matrices as model systems for the fuel cells technology.

We showed that the functional properties (thermal stability, conductivity) are strongly dependent on microstructural parameters like tortuosity and pores size distribution, and cannot be simply rationalized in terms of the maximum available pore size.

Generally speaking, the solution absorbed into these matrices is not completely free to flow, but must be treated as a partially confined liquid also in the case of nominal pore sizes in the micrometer range. Both the interactions among the various solution components and among the ions and the polymer strands are not negligible, and must be taken into account in the design of nano-composite systems with passive or even active fillers.

Acknowledgement

This work has been financially supported by MIUR (FISR 2001) under the NUME project “Sviluppo di membrane protoniche composite e di configurazioni elettrodiche innovative per celle a combustibile con elettrolita polimerico”.

References

[1] O. Savadogo, J. Power Sources 127 (2004) 135.
[2] B. Gupta, G.G. Scherer, J. Appl. Polym. Sci. 50 (1993) 2159.
[3] B. Gupta, F.N. Buchi, M. Staub, D. Gurman, G.G. Scherer, J. Polym. Sci., Part A: Polym. Chem. 34 (1996) 1873.
[4] B. Gupta, F.N. Buchi, G.G. Scherer, Polym. Adv. Technol. 5 (1994) 493.
[5] B. Gupta, G.G. Scherer, Chimia 48 (1994) 127 (reference cited therein).
[6] H.P. Brack, H.G. Buherer, L. Bonorand, G.G. Scherer, J. Mater. Chem. 10 (2000) 1795.
[7] S. Holmberg, J. Nasman, F. Sundholm, Polym. Adv. Technol. 9 (1998) 121.
[8] T. Lehtinen, G. Sundholm, S. Holmberg, F. Sundholm, P. Bjornbom, M. Bursell, Electrochim. Acta 43 (1998) 1881.
[9] S. Holmberg, P. Holmlund, R. Nicolas, C.-E. Wilen, T. Kallio, G. Sundholm, F. Sundholm, Macromolecules 37 (2004) 9909.
[10] N. Walsby, F. Sundholm, T. Kallio, G. Sundholm, J. Polym. Sci., Part A: Polym. Chem. 39 (2001) 3008.
[11] T. Kallio, C. Slevin, G. Sundholm, P. Holmlund, K. Kontturi, Electrochem. Commun. 5 (2003) 561.
[12] T. Kallio, K. Jokela, H. Ericson, R. Serimaa, G. Sundholm, P. Jacobsson, F. Sundholm, J. Appl. Electrochem. 33 (2003) 505.
[13] T. Kallio, M. Lundstrom, G. Sundholm, N. Walsby, F. Sundholm, J. Appl. Electrochem. 32 (2002) 11.
[14] B. Soresi, E. Quartarone, P. Mustarelli, A. Magistris, G. Chiodelli, Solid State Ionics 166 (2004) 383.
[15] X. Qiu, Z. Wenqiong, S. Zhang, H. Liang, W. Zhu, J. Electrochem. Soc. 150 (2003) A917.
[16] L. Gubler, S.A. Gürsel, G.G. Scherer, Fuel Cells 5 (2005) 317.
[17] A.S. Gozdz, C. Schumutz, J.M. Tarascon, P.C. Warren, US Patent 5,296,318 (1995).
[18] E. Quartarone, P. Mustarelli, A. Magistris, J. Phys. Chem. B 106 (2002) 10828.
[19] E. Peled, T. Duvdevani, A. Melman, Electrochem. Solid State Lett. 1 (1998) 210.
[20] M.A. Navarra, S. Materazzi, S. Panero, B. Scrosati, J. Electrochem. Soc. 150 (2003) A1528.
[21] M.A. Navarra, S. Panero, B. Scrosati, J. Solid State Electrochem. 8 (2004) 804.
[22] H. Strathmann, K. Kock, Desalination 21 (1977) 241.
[23] G. Alberti, M. Casciola, Annu. Rev. Mater. Res. 33 (2003) 129.
[24] M. Casciola, G. Alberti, A. Ciarletta, A. Cruccolini, P. Piaggio, M. Pica, Solid State Ionics 176 (2005) 2985.
[25] N.A. Ochoa, P. Prasanos, L. Palacio, C. Pagliero, J. Marchese, A. Hernandez, J. Membr. Sci. 187 (2001) 237.
[26] See technical FAQs at http://www.millipore.com.
[27] M. Khayet, K.C. Khulbe, T. Matsuura, J. Membr. Sci. 238 (2004) 199.
[28] X. Ren, T.E. Springer, T.A. Zawodzinki, S. Gottesfeld, J. Electrochem. Soc. 147 (2000) 466.
[29] M.W. Verbrugge, J. Electrochem. Soc. 136 (1989) 417.
[30] J.P. Shin, B.J. Chang, J.H. Kim, S.B. Lee, D.H. Suh, J. Membr. Sci. 251 (2005) 247.
[31] M. Sahimi, Rev. Mod. Phys. 65 (1993) 1393.
[32] K.R. Jeffrey, G.Z. Zukowska, J.R. Stevens, J. Chem. Phys. 119 (2003) 2422.